1-1999

Five Myofibrillar Lesion Types in Eccentrically Challenged, Unloaded Rat Adductor Longus Muscle—A Test Model

Joyce L. Thompson
Medical College of Wisconsin

Edward Michael Balog
Marquette University

Robert H. Fitts
Marquette University, robert.fitts@marquette.edu

Danny A. Riley
Medical College of Wisconsin

The Anatomical Record, Vol. 254, No. 1 (January 1, 1999): 39-52. DOI.

Five Myofibrillar Lesion Types in Eccentrically Challenged, Unloaded Rat Adductor Longus Muscle—A Test Model

Joyce L. Thompson
Cell Biology, Neurobiology & Anatomy, Medical College of Wisconsin, Milwaukee, WI
Edward M. Balog
Department of Biology, Marquette University, Milwaukee, WI
Robert H. Fitts
Department of Biology, Marquette University, Milwaukee, WI
Danny A. Riley
Cell Biology, Neurobiology & Anatomy, Medical College of Wisconsin, Milwaukee, WI
Cell Biology, Neurobiology & Anatomy, Medical College of Wisconsin, Milwaukee, WI

Abstract

Sarcomere disruptions are observed in the adductor longus (AL) muscles following voluntary reloading of spaceflown and hindlimb suspension unloaded (HSU) rat, which resemble lesions in eccentrically challenged muscle. We devised and tested an eccentric contraction (ECCON) test system for the 14-day HSU rat AL. Six to 7 hours following ECCON, ALs were fixed to allow immunostaining and electron microscopy (EM). Toluidine blue-stained histology semithin sections were screened for lesion density (#/mm^2). Serial semithin sections from the ECCON group were characterized for myosin immunointensity of lesions. Five myofibrillar lesion types were identified in histological semithin sections: focal contractions; wide A-bands; opaque areas; missing A-bands; and hyperstretched sarcomeres. Lesion density by type was greater for ECCON than NonECCON ALs ($P \leq 0.05$; focal contractions and opaque regions). Lesion density (#-of-all-five-types/mm^2) was significantly different (ECCON: 23.91 ± 10.58 vs. NonECCON: 5.48 ± 1.28, $P \leq 0.05$; ECCON vs. SHAM: 0.00 ± 0.00; $P \leq 0.025$). PostECCON optimal tension decreased (Poi-drop, 17.84 ± 4.22%) and was correlated to lesion density (R^2 = 0.596), but prestretch tension demonstrated the highest correlation with lesion density (R^2 = 0.994). In lesions, the darkly staining A-band lost the normally organized thick filament alignment to differing degrees across the different lesion types. Ranking the five lesion types by a measure of lesion length deformation (hypercontracted to hyperstretched) at the light microscopy level, related to the severity of thick filament registry loss across the lesion types at the electron microscopic level. This ranking suggested that the five lesion types seen in semithin sections at the light level represented a lesion progression sequence and paralleled myosin immunostaining loss as the distorted A-band filaments spread across the hyperlengthening lesion types. Lesion ultrastructure indicated damage involved calcium homeostasis loss (focal contraction lesions) and "thick-filamentcentering" failure of titin (wide A-band lesions) in the early stages of lesion development. Anat Rec 254:39–52, 1999. © 1999 Wiley-Liss, Inc.

Morphological examination of atrophic muscles from rats which had been unloaded by either microgravity exposure during spaceflight or hindlimb suspension unloading (HSU) and subsequently reloaded have shown lesions (Riley et al., **1990**, **1992**, **1995**, **1996a**). These lesions resembled those produced by eccentric (lengthening; pliometric) contractions[1] in animals and man, i.e., sarcomere focal hyperwidening, myofilament loss, misalignment, and complete breakdown (Friden et al., **1983**, **1988**; Sjostrom and Friden, **1984**; Newham et al., **1983**; McCully and Faulkner, **1985**, **1986**; Ogilvie et al., **1988**; Friden and Lieber, **1992**; Wood et al., **1993**; Lieber and Friden, **1993**; Watchko et al., **1994**; Hunter and Faulkner, **1996**; MacPherson et al., **1996**). The affected myofibers occur in groups rather than randomly or scattered (Thompson, **1994**). This suggests that during active pliometric-induced mechanical failure there is either fiber–fiber interaction or a spreading of damage from focal disruptions within the muscle. The importance of the eccentric component in this scenario is further suggested by the greater lesion frequency (41.5 ± 9.8% fibers affected; Riley et al., **1992**) after high-G impact parachute reentry of Cosmos biosatellites, than the lower frequency (<5.5% fibers affected) following low-G runway landing of the Spacelab and Life Sciences Mission (SLS-2; Riley et al., **1996**). No lesions were observed in the atrophic muscles removed from rats in microgravity (no reloading) during the SLS-2 mission.

For normal (1G adapted) muscles, it has been recognized by numerous investigators that eccentric (lengthening or pliometric) contractions are more damaging than isometric or concentric contractions (McCully and Faulkner, **1985**; Gibala et al., **1995**; Brooks et al., **1995**; Watchko et al., **1994**; Warren et al., **1994**; Lieber and Friden **1993**; Lieber et al., **1991**; Hutchens and Skjonsby, **1990**; Wood et al., **1993**; Ogilvie et al., **1988**; Armstrong et al., **1983**; Friden et al., **1983**; Newham et al., **1983**; Schwane and Armstrong, **1983**). Eccentric contractions generate higher total work and tension at equal strain and strain rate than concentric contractions and are consistently associated with reductions in tetanic tension following treatment (Lieber and Friden, **1993**; Lieber et al., **1991**). This immediate reduction in tension has served as the hallmark of muscle damage following eccentric treatment of normal muscle (MacPherson et al., **1996**; Gibala et al., **1995**; Warren et al., **1994**, **1993**a,**b**; McCully and

Faulkner **1985**, **1986**). These observations are consistent with the hypothesis that microgravity unloading removes the eccentric component and renders postural muscles susceptible to eccentric contraction damage upon reloading (Hargens et al., **1989**). However, it has not been established whether myofibrillar lesion damage is due to the higher tensions at reload (simple overload: increased body mass to muscle mass ratio following atrophy; no change in myofibrillar damage threshold) or to a lowered myofibrillar injury threshold, which in the atrophic state may allow myofibrillar damage at lower tension per cross-sectional area. Before the impact of the eccentric component in reload damage to the microgravity or simulated microgravity adductor longus (AL) could be evaluated, a test system had to be devised to accommodate the atrophic AL. The eccentric contraction and tendon reattachment model pioneered by McCully and Faulkner (**1985**, **1986**) for normal extensor digitorum longus (EDL) muscle was adapted for the atrophic rat AL muscle (Thompson, **1993**) and evaluated for its ability to replicate volitional reload damage. We further characterize the histology, myosin immunostaining properties and ultrastructure of the lesions produced by this model under known tension for atrophic adductor longus.

MATERIALS AND METHODS

Animal Model

The rat AL muscle was chosen for study because it has previously been shown to atrophy during unloading (30%) and manifest sarcomeric lesions after reloading (20–70% fibers affected; Riley et al., **1996**, **1995**, **1992**; Krippendorf and Riley, **1994**). This muscle is postural, and a prime mover in the power stroke of running and swimming (Roy et al., **1985**). The AL originates along the ascending ramus of the symphysis pubis and inserts just lateral to the pectineus, at a point one-third the length from the proximal end of the femur (Popesko et al., **1990**). Figure **1** shows the actions about the hip joint produced by contraction of the AL. The long slender insertion tendon facilitates surgical attachment to force transducers, as well as reattachment to the distal stump for long-term repair studies. Additionally, the AL muscle has a fiber type composition similar to the soleus, but the fast twitch oxidative glycolytic (FOG) fibers are concentrated in the rostral one-third of the muscle (soleus: (FOG/SO%): 20/80, Armstrong and Phelps, **1984**; AL (FOG/SO%): 15/85, Riley et al., **1995**). This facilitates examination of a practically pure slow twitch oxidative (SO) population. In all cases the animals were treated in accordance with the PHS Guidelines for Care and Use of Laboratory Animals (NIH PUB No. 86–23). The rats were maintained on a diet of Purina Rat Chow and water ad libitum, under a 12 hour on/off light cycle.

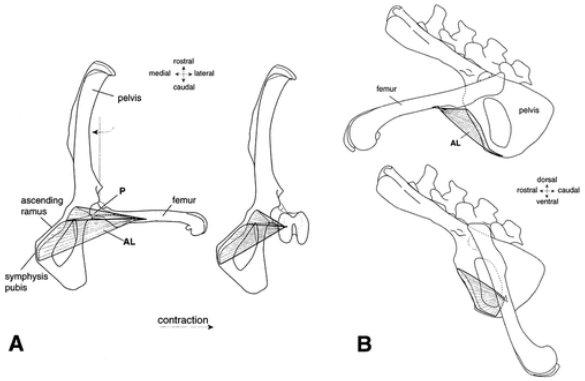

Figure 1: Ventral view of the left rat pelvic bone (**A**) showing the location of the adductor longus (AL) and pectineus (P) with the femur in two positions: abducted (left) and adducted (right). The lateral view (**B**) of pelvis shown with femur in two positions: flexed (top) and extended (bottom). AL origin: from the anterior portion of the symphysis pubis and along the caudal two-thirds of the ascending ramus. AL insertion: the distal tendon becomes common with the distal portion of the pectineus tendon and inserts on the posterio-medial surface of the femur shaft, approximately at the shaft midpoint. AL action: femur adduction and extension; active in the power stroke (femur extension) of running and swimming (Roy et al., **1985**).

Hindlimb Suspension Unloading (HSU)

The animals underwent 14 days of HSU, according to Fitts et al. (**1986**). The 14-day time period was selected to coincide with previous suspension work and the Cosmos 1887 and 2044 missions (Krippendorf and Riley, **1994**; Riley et al., **1990**, **1992**). Briefly, the animals' rear feet were held just off the cage floor by a sling wrapping the proximal two-thirds of the tail. A swivel, anchored to a fixed point above the cage, was attached to the distal end of the harness to allow freedom of movement and access to food and water.

Eccentric Contraction (ECCON) Protocol

HSU rats were anesthetized with pentobarbital (i.p., 40 mg/Kg) and rectal temperature was maintained at 36.5°C with a heating mat and Yellow Springs thermoregulator. The skin in the inguinal region was shaved and cleaned with alcohol and Betadine. The AL muscle was exposed via a skin incision, and its distal tendon isolated by blunt dissection. A Kessler knot of 8.0 blue monofilament ligature for eventual reattachment was placed in the tendon prior to severing the distal insertion. The distal tendon was attached to a force transducer—servomotor (Cambridge Technologies, Inc., Cambridge, MA) via a 6.0 braided silk suture. The angle of pull for the AL was along the femur placed at 90° flexion at the hip (Fig. **1**). The direction of muscle pull was set 10° less than full abduction of the femur in order for the transducer arm to clear the knee joint. The pelvis and femur were stabilized with bone clamps. Blood flow to the AL muscle was maintained by sparing the muscle vasculature. The experimental setup is diagrammed in Figure **2**.

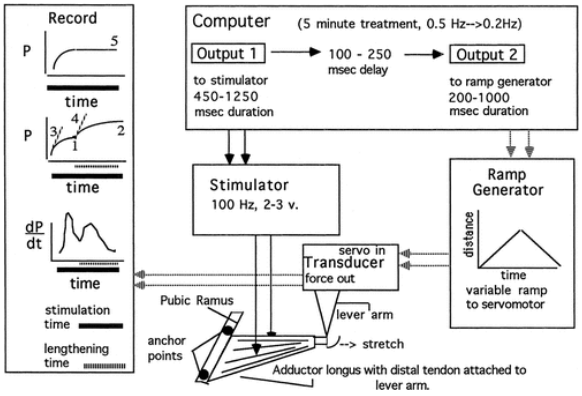

Figure 2: Schematic of the system designed to produce eccentric contractions in the adductor longus. The computer outputs a signal to the muscle stimulator (Output 1) and, after a specified delay, activates the triangle wave generator (Output 2) to the servomotor unit (Cambridge force transducer — servomotor). The rate and duration of the "strain" produced by the servomotor are determined by the slope and amplitude of the triangle wave. Tension (P; "stress") output from the force transducer is recorded by the computer for later determination of P and dP/dt. Tension trace key positions and abbreviations: 1, Pbeg-str: begin stretch tension; 2, Pend-str: end stretch tension; 3, dPtetanus/dt: maximum rate of tension increase per time during tetanic contraction; 4, dPstretch/dt: maximum rate of tension increase per time during active lengthening; 5, Poi: preECCON or initial optimal tetanic tension.

The employed eccentric (pliometric) contraction (ECCON) protocol was modified from that of McCully and Faulkner (**1985**, **1986**), because pilot testing demonstrated that their faster stretch protocols for normal muscles were too damaging to atrophic muscle. Two stimulating platinum electrodes (~1.5 × 6 mm) were placed on the dorsal and ventral surfaces of the muscle over the endplate region. This placement avoided compression of blood vessels. Satisfactory positioning of the electrodes only evoked AL contractions. Initial optimal tension (Poi) and optimal length (Loi) were determined. One hundred lengthening contractions were performed at 20 contractions/min for a period of 5 min. Muscles were supramaximally stimulated with 3 V at 100 Hz for 500 msec total duration; lengthening duration was 400 msec and lengthening distance was 2 mm (mean±SEM,

1.083±0.0028 Lo; Rate, 0.208±0.0071 Lo/s). Tension was recorded every 30 sec during the ECCON treatment. Fifteen minutes after ECCON, Po was remeasured to detect drops in Poi (Poi-drop). Maximum tetanic tension in normal muscle recovered from a 5 min tetanic contraction within 10 min. Decreases in Po relative to Poi persisting after the 15-min rest were attributed to the ECCON treatment rather than fatigue. Test muscle desiccation was prevented by a Krebs-Ringer drip and application of a sterile plastic drape. Upon completion of the ECCON treatment, the tendon was reattached to the remaining distal stump on the femur via 8.0 Prolene and a second Kessler knot, and the skin incision closed. When conscious, the animal was returned to his cage to simulate the Cosmos 2044 mission reloading. Muscles were sampled 6.9±0.3 hr post-ECCON for a total reload time of 3.6±0.2 hr on awakening from anesthesia.

Tissue Processing

Rats were anesthetized with sodium pentobarbital (40 mg/kg, i.p.). The ECCON and NonECCON AL muscles were excised, and the animals were euthanized by anesthetic overdose and pneumothorax. Isolated muscles were weighed. A 1.5–2 mm thick strip was cut from the caudal border of the muscles (slow twitch oxidative region) and pinned out under mild stretch of 1.1–1.2 Lo in Krebs-Ringer physiological buffer. The required stretch of the muscle strip was determined via a mm ruler from two fiducial points established while the muscle was on the force transducer at Lo. This region was examined because previous work indicated that 95% of lesions occurred caudally (Krippendorf and Riley, **1994**). The tissue was fixed in 4% paraformaldehyde, 0.1% glutaraldehyde in 100 mM phosphate, pH 7.4, for 2 hr at 4°C. Following four rinses (100 mM phosphate buffer, pH 7.4) tissues were dehydrated in graded ethanols and sequentially infiltrated with ethanol/LR White mixtures (2:1 and 1:2 for 1 hr each). After three changes in 100% LR White over 24 hr, specimens were embedded in airtight gelatin capsules at 60°C overnight. Comparable regions were obtained from surgical shams (SHAM, n = 6) and processed in the same manner, following tendon isolation and mock transducer attachment.

Light Microscopy Lesion Morphology

Longitudinal, 0.5 µm, LR White sections were cut (Reichert Ultracut, Austria) from the AL caudal midbelly of ECCON-treated, NonECCON-treated, and surgical sham (SHAM)-treated animals. The semithin sections were collected on glass slides and stained with aqueous toluidine blue (0.5% toluidine blue in 0.5% borax) at 80°C, rinsed in distilled water, and dried on the hotplate before mounting in Permount.

The total number of lesions and numbers of lesions by type (defined in **Results**) were recorded and normalized to contractile area ("lesion density" and "lesion density by type"; #/mm^2) by measuring the toluidine-positive area of each section on a Nikon Optiphot microscope using Bioquant digitizing software (R and M Analysis, Knoxville, Tennessee). Lesion density and lesions density by type were similarly quantified in sections of AL muscles from a previous HSU-reload study (12.5-day HSU; 0, 6, and 12 hr reload; Krippendorf and Riley, **1994**).

Lesions vary in size from small to large and in sarcomeric length deformation from hypercontracted to hyperstretched, so measurements to segregate these parameters were employed. Lesion size was defined as number of sarcomeres involved in a lesion (#Sarcs) and reported as the range in #Sarcs for a lesion type. This was more informative than absolute length (µm) and area (µm^2), which were greatly affected by the severity of lesion hypercontraction or hyperstretch. In LM photomicrographs, the degree of sarcomere length deformation for whole lesions was expressed as "lesion deform ratio" (LDR), which was the total lesion length divided by the length of an equal number of nonlesioned sarcomeres from an intact region. In all lesioned areas enough remnants of sarcomeric detail remained for an accurate #Sarcs count.

LM Immunostaining Characteristics of Lesions

Semithin sections serial to the toluidine blue histological sections were dried onto chromalum-coated glass slides (0.05% chromium potassium sulfate in 0.5% gelatin) for immunohistochemical staining. After blocking 20

min with 2% normal goat serum (w/v), sections were treated with a 1/30 dilution (v/v) of antimyosin primary antiserum (Sigma polyclonal antibody #7523; stains skeletal muscle myosin heavy and light chains in animal muscle, but not smooth muscle) for 2 hr at room temperature followed by overnight incubation at 4°C. Unbound primary antibody was removed by three 10-min rinses in 100 mM phosphate buffer (pH 7.4). Bound primary antibody was visualized by incubation in FITC-conjugated goat anti-rabbit IgG secondary antibody (1:50 dilution (v/v) overnight). Unbound secondary antibody was removed by rinsing three times in the phosphate buffer. Nonspecific binding of secondary was detected by omission of the primary antibody. The relative immunointensities of the five lesion types (defined in **Results**) were visually evaluated from identically exposed and processed negatives and photomicrographs.

EM Lesion Ultrastructure

Examples of each of the five types of lesions were localized in semithin sections. Blocks were trimmed to ultrathin section for the lesions of interest. Silver to white gold sections were collected on formvar-coated nickel grids and postfixed with vapors from a 1% aqueous osmium tetroxide solution at room temperature (1 hr), then rinsed in distilled water. Following counterstaining in lead citrate (2.8%, w/v) and uranyl acetate (5.0%, w/v), sections were examined and photographed with a JEOL CX100 electron microscope. In electron micrographs, the sarcomeric deformation for individual sarcomeres in each of the five lesion types was measured and designated as “sarcomeric deform ratio” (SDR). The SDR was the length of a lesioned sarcomere divided by the length of a nearby intact sarcomere.

Statistical Tests

Unless otherwise stated, values are mean ±SEM. The Wilcoxon Paired Sample Test and Mann-Whitney U-Test were used to detect pairwise differences for lesion density in ECCON-treated vs. NonECCON-treated HSU muscles, and ECCON-treated vs. SHAM-treated muscles.

Lesion density across the ECCON-treated muscles was correlated with the following physiological parameters from the initial lengthening cycle for each of the muscles: tension at the beginning of stretch (Ppre-str); tension at the end of stretch (Pend-str); dPtetanic/dT; dPstretch/dT; Work; Poi-drop; and body weight to muscle weight ratio (Wb:Wm ratio). The rank correlations were conducted by Spearman's Rank Correlation Coefficient (r_S; Hewlett Packard StatPac 1; Corvallis, OR) and tested for independence of lesion density and the respective physiologic parameters (Z statistic, $P \leq 0.05$; calculated from the r_S value; Hewlett-Packard StatPac 1; Corvallis, OR). The coefficient of determination (R^2) for each scatter plot between the lesion density and the respective physiological parameter was determined for the least squares line ($y = mx + b$). This value indicates the percentage of variation in lesion density within the muscles that was explained by the respective physiological parameter recorded on these muscles (Zar, **1974**).

RESULTS

Lesion Morphology and Immunostaining

At the LM level, five morphological types of sarcomere lesions were defined on the basis of appearance in toluidine blue-stained, semithin sections of LR White embedded tissues: focal contraction (FC), wide-A band (WID-A), opaque region (OPAQ), missing-A band (MIS-A) and hyperstretched region (HS). The lesion types are illustrated in Figure **3**A–E; lesion density by type for the HSU ECCON treatment rats and the HSU-reloaded rats are given in Figure **4**A and B, respectively. The same morphological types of lesions were identifiable in the ECCON-treated AL and the HSU-reloaded AL muscles from Krippendorf and Riley (**1994**).

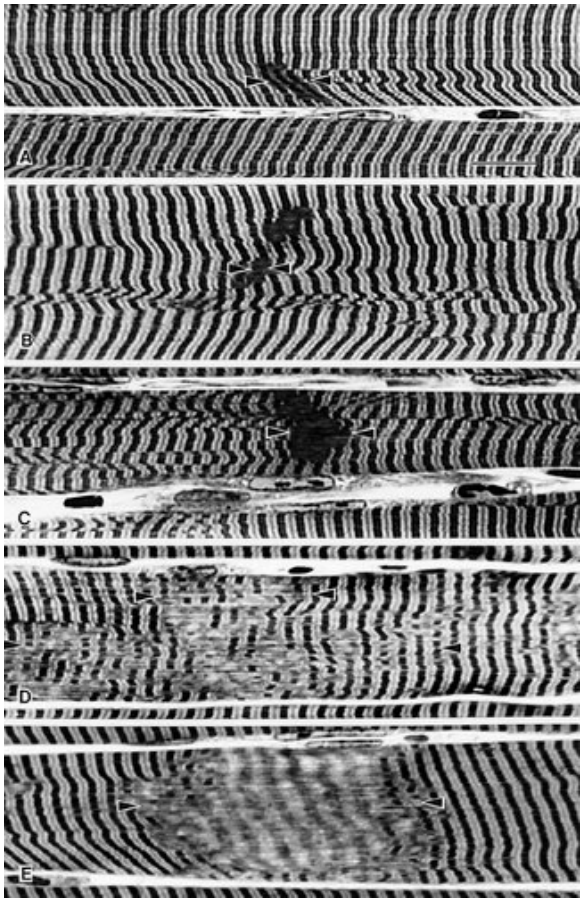

Figure 3 Morphology of the lesion types seen following the eccentric challenge to atrophic AL muscle. The same lesion types were present in volitionally reloaded 12.5-day HSU muscle, but not in the SHAM muscle. Toluidine blue-stained semithin sections of LR White embedded tissue. LDR: lesion deform ratio (±SD); #Sarcs: range in number of sarcomeres within the lesion type. Black-white bar equals 10 μm. (**A**) Focal contraction (FC) lesion. These areas show myosin bands which are frequently thinner and less intensely toluidine blue-stained than those in the surrounding nonlesioned areas. The involved Z-lines frequently exhibit some waviness. Deform ratios are reduced; LDR = 0.510 ± 0.157; #Sarcs = 3–15. (**B**) Wide A-band (WID-A) lesions. Morphologically, these lesions extend from one Z-line to an adjacent Z-line with a thickness of from 1 to 6 μm and stain darkly with toluidine blue. They mostly occur singly and demonstate angular corners. LDR = 0.986 ± 0.019; #Sarcs = 1–2. (**C**) Opaque region (OPAQ) lesions. These lesions involve several sarcomeres and stain darkly in toluidine blue, similar to the WID-A lesion. Generally, OPAQs show slightly wider deform ratios and more rounded edges. LDR = 1.023 ± 0.050; #Sarcs = 2–5. (**D**) Missing A-band (MIS-A) lesions. In these lesions the toluidine blue-stained A-bands appear abruptly missing. The lesion may or may not be associated with hyperlengthening of the associated sarcomeres. LDR = 1.023 ± 0.051; #Sarcs = 1–18. (**E**) Hyperstretched sarcomere (HS) lesions. These lesions are characterized by extreme lengthening, diminished toluidine blue staining of sarcomere cross-striations, and often loss or disruption of the Z-lines. LDR = 1.380 ± 0.205; #Sarcs = 1–16.

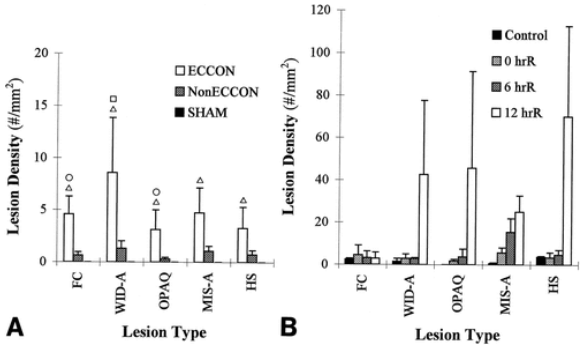

Figure 4 Bar graph depicting the lesion density by type (**A**) in the 3–4 hr reloaded ECCON, the contralateral 3–4 hr reloaded NonECCON, and the surgical SHAM muscles (no lesions). Abbreviations as in Fig. **3**. Symbols denote a significant difference between ECCON and NonECCON muscles (circle, $P \leq 0.05$; square, $0.05 \leq P \leq 0.075$) and ECCON and SHAM (triangle, $P \leq 0.025$) via Wilcoxon paired sample test and Mann-Whitney U-test; n = 6 per group (error bars denote SEM). One NonECCON muscle demonstrated widespread evidence of anoxic necrosis not present in the other five NonECCON muscles, the six ECCON muscles, or the six SHAM muscles. This muscle was the last of the pair to be isolated during the second anesthesia (35 min). HSU rats are extremely susceptible to anesthesia overdose on multiple exposure and this morphology suggests circulatory compromise to this NonECCON muscle. The average lesion density by type value for the other five NonECCON muscles was used for statistical calculations (n = 6). All lesion types are exaggerated in the ECCON-treated muscle over the NonECCON-treated muscle and lesion density (#-all lesion-types/mm^2) ECCON (n = 6) is greater than NonECCON (n = 5) via Mann Whitney U-test, $P \leq 0.05$. (**B**) Lesion density by type in the AL of rats volitionally reloaded following 12.5 days of HSU treatment (n = 2/timepoint; 0, 6, and 12 hr reload, #hrR; tissue from Krippendorf and Riley, **1994**). Rats performed forceful, reflexive kicking on sacrifice by guillotining under anesthesia, so baseline levels may be slightly elevated. The lesion types progress together except for the FC type, and all lesion types seen in the ECCON tissue are mirrored in the volitionally reloaded, 12.5 day HSU rat, evidencing a similar eccentically induced formation mechanism.

Intact sarcomeres from both normal and HSU muscle fixed under moderate stretch, 1.1–1.2 Lo, have wide, very dark A-bands, thin moderately stained Z-lines, and wide lightly stained I-bands in toluidine blue-stained, LR White, semithin sections (Figs. **3**, **5**A_1, B_1, C_1, D_1, E_1). Immunofluorescence staining for sarcomeric myosin in sections serial to the toluidine blue sections show brightly reactive A-bands alternating with nonstained dark I-bands, revealing the normal cross-striated arrangement of the contractile proteins (Figs. **5**A_2, B_2, C_2, D_2, E_2).

FC lesions, at the LM level, were focal areas of hypershortened sarcomeres in which the I-bands were shortened to varying degrees and the A-bands were narrowed (Figs. **3**A, **5**A_1). Sarcomeric myosin immunostaining was only slightly decreased (Fig. **5**A_2). FC lesions exhibited a great degree of ultrastructural variation, both in extent of sarcomere disorganization and individual deformation ratios, ranging from mildly contracted (SDR, 0.8) to severely shortened (SDR, 0.5). In mildly contracted lesions, Z-lines were wavy and showed diminished electron opacity, and thick filaments showed minor lateral displacement. In the severely affected sarcomeres, there was marked Z-line dissolution, as well as loss of and lateral displacement of thick filaments. The morphological appearance was consistent with variable calcium-activated proteolysis (Duncan, **1987**, **1989**).

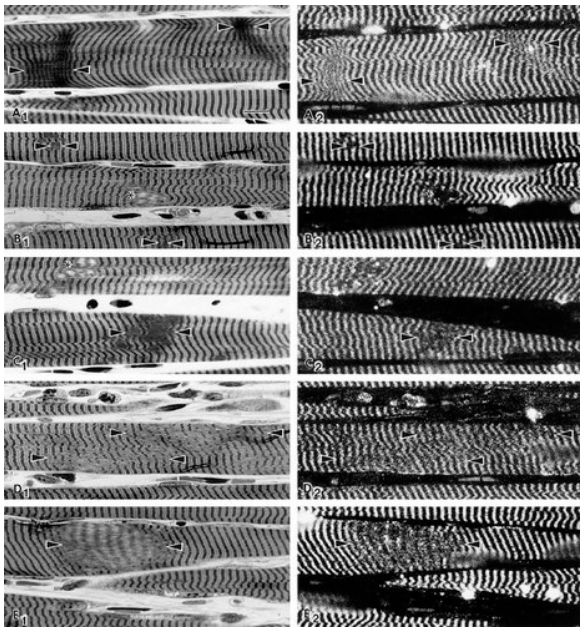

Figure 5 Toluidine blue (1) and pAbM7523 stained (2) serial sections. The lesion types marked by black-white arrowheads are as follows: FC lesion (**A_1, A_2**); WID-A lesion (**B_1, B_2;** an asterisk marks a small HS lesion); OPAQ lesion (**C_1, C_2;** an asterisk marks a small HS lesion); MIS-A (**D_1, D_2**); and HS lesion (**E_1, E_2**). There is a progressive loss in myosin staining across the FC, MIS-A, and HS lesion types (A_2, D_2, E_2, respectively), which parallels the diminished toluidine blue staining of the myosin and the increase in LDR values across these lesion types (A_1, D_1, E_1, respectively). However, the WID-A and OPAQ lesion types show almost complete loss of myosin immunostaining (B_2, C_2) despite LDR values near unity and relatively dark toluidine blue staining of the lesions (indicative of myosin presence; B_1, C_1). Less immunomyosin loss placed FC lesions before MIS-A and HS lesion types. The severe immunomyosin loss, large SDR (see Fig. **6**), and digested appearance place HS lesions after the other four with MIS-A lesion type in between, generating a lesion development sequence as follows: FC to MIS-A to HS. Despite the lack of immunomyosin staining, EM evidence (see Fig. **6**) places WID-A and OPAQ lesions early in the proposed progression sequence, ahead of the MIS-A lesion type. Black-white bars equals 10 μm.

WID-A lesions, in toluidine blue LM sections, were abrupt, focal areas in which the darkly stained A-band of a sarcomere extended from Z-line to Z-line, giving the appearance that the A-band had expanded the full width of the sarcomere. These lesions most often occurred as single sarcomeres, but small clusters of two consecutive sarcomere were seen. The outer border was “boxy” as opposed to a “smooth curve.” The toluidine blue staining intensity of a WID-A lesion was slightly less dense than a nonlesioned A-band (Figs. **3**, **5**B_1). WID-A lesions exhibited little or no sarcomeric myosin immunostaining (Fig. **5**B_2). At the EM level, WID-A lesions or clusters were characterized by laterally displaced thick filaments which intruded into the I-band and contacted the relatively intact Z-lines (Fig. **6**B). M-lines were missing, indicating loss of lateral anchoring of thick filaments. Sarcomere deformity ranged from none to very mild in most cases (SDR, 1.0–1.1).

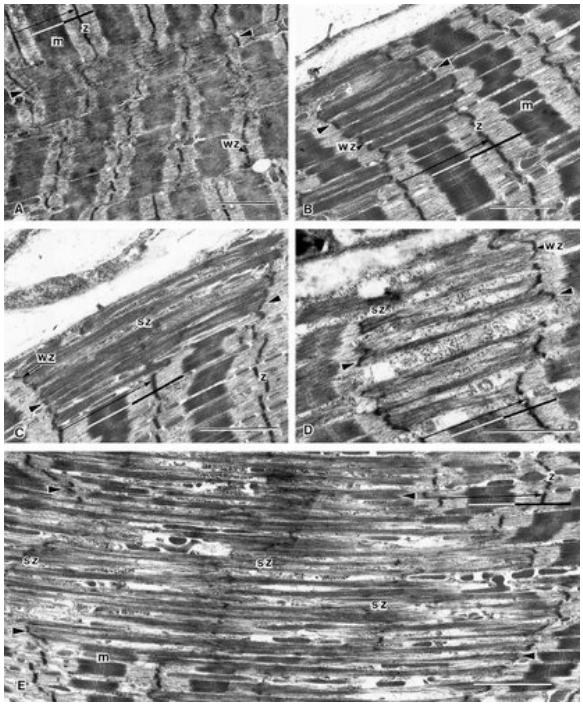

Figure 6 Abbreviations: z, Z-line; sz, streaming Z-line; wz, wavy Z-line; m, m-line; thick white bar, A-band; thick black bar, I-band; thin black arrow, one sarcomere; black-white arrowheads, enclose lesion; SDR, sarcomere deform ratio; Black-white bars at lower right equal 2.0 μm. (**A**) Ultrastructure of the FC lesion type. Note the narrow I-bands and reduced SDR values (0.7–0.8). (**B**) Ultrastructure of the WID-A lesion type. There is "thick-filament-lateral-slippage" to the Z-lines with minimal Z-disk disruption (SDR range: 1.0–1.1). (**C**) A small OPAQ lesion. Progressive thick-filament-slippage with marked Z-line disruption is apparent as the SDR increases (1.0–1.4). The Z-disk within the lesion shows considerable streaming and dissolution, typical of the larger OPAQ lesions. (**D**) A MIS-A lesion type. There is severe thick-filament-slippage in the single hyperwidened sarcomere, with prominent wavy and streaming Z-lines (SDR range: 1.0–1.6, approaching that seen in HS lesions). (**E**) A montage of the HS lesion type covering three sarcomeres. The entire lesion exhibits extreme thick-filament-slippage with prominent Z-line streaming and dissolution. SDR range: 1.6–2.5.

OPAQ lesions at LM level appeared to be large clusters of WID-A lesions, involving more sarcomeres in the transverse and longitudinal dimensions (Fig. **3**C). Like WID-A's, the OPAQ lesions also had markedly reduced immunostaining for sarcomeric myosin (Fig. **5**C_2), and dark toluidine blue intensity (Fig. **5**C_1). Unlike WID-A lesions, the perimeter of OPAQ lesions seemed a smoother curve, rather than boxy. At the EM level, the core of the OPAQ lesion exhibited smeared Z-line-like material, and the lesion periphery showed intact but wavy Z-lines. Examples of transitional WID-A's/OPAQ's (two sarcomeres long) with no deformation on one edge of the lesion and deformation on the other end were also found (Fig. **6**C; SDR, 1.1–1.4). As in the OPAQ lesions, in such two-sarcomere-long WID-A/OPAQ transition lesions, the Z-line within the lesion appeared degraded, whereas those at the ends were more normal in appearance.

MIS-A lesions at the light level were sites in which A-band staining was absent in toluidine blue-stained sections, producing a broken pattern of transverse striations with the average sarcomere spacing relatively normal (Figs. **3**D, **5**D_1). This patchy banding pattern involved from one to 20 sarcomeres. The transverse immunofluorescent myosin bands were disrupted and reduced in intensity in the areas of MIS-A lesions (Fig. **5**D_2). At the electron microscopic level, MIS-A lesions were characterized by a major loss of sarcomere structure over a few sarcomeres with relatively normal ones interspersed within the lesion. In the most affected sarcomeres, the few remaining bundles of thick filaments were displaced to the Z-lines and separated by large areas of cytoplasm, M-

lines were absent, and Z-lines were periodically missing or wavy in appearance (Fig. **6**D). Thin filaments were also reduced in number. These regions of reduced electron-dense structures appeared to be the early stages of the more uniformly severe sarcomere degradation characteristic of HS lesions (see below).

HS lesions at the LM level were large foci of hyperstretched sarcomeres with wider, diffuse A-bands showing diminished toluidine blue staining (Figs. **3**E, **5**E_1) and markedly reduced sarcomeric myosin immunoactivity (Fig. **5**E_2), suggesting a major thinning and shifting of A-band components. HS lesion ultrastructure was characterized by widely dispersed Z-line remnants, severely displaced thick filaments, and a very large sarcomere deformation ratio ($1.6 \leq SDR \leq 2.5$) uniformly continuing from 1–16 sarcomeres. Unlike the MIS-A lesions, relatively normal sarcomeres did not occur within the HS lesion. The remnants of Z-lines with associated thick and thin filaments were widely separated, creating large areas of electron-lucent cytoplasm (Fig. **6**E).

Lesion Parameters

The lesion density was significantly greater ($P \leq 0.05$, Wilcoxon Paired Sample Test and Mann Whitney U-test; n = 6/group) in the ECCON-treated group (23.9 ± 10.6 lesions/mm^2) than the NonECCON-treated group (5.5 ± 1.3 lesions/mm^2). SHAM-treated muscles had no lesions and were also significantly different from the ECCON group ($P \leq 0.025$). Within the ECCON group, there were wide variations in lesion density and lesion density by type, despite similar maximum endstretch tensions. All lesion types were more prevalent on the treated side than the contralateral NonECCON muscles, with FC and OPAQ lesion types significantly higher ($P \leq 0.05$; Mann-Whitney and Wilcoxon; Fig. **4**A).

Mean lesion sizes as "number of sarcomeres in lesion types" (#Sarcs) increased as follows: WID-A << OPAQ ≤ FC < MIS-A ≋ HS, with the MIS-A and HS types showing the most variation. The LM lesion deformity, as LDR (mean ±SD), increased as follows: FC (0.510±0.157) << WID-A (0.986±0.019) ≤ OPAQ (1.023±0.050) ≤ MIS-A (1.023±0.051) << HS (1.380±0.205), with the FC and HS types having the largest variation (Fig. **3**). Ultrastructurally, SDR ranges for each lesion type paralleled the LDR ranges, although the SDR ranges for MIS-A and HS lesions were much larger (Fig. **6**.).

Physiological Responses to ECCON Treatment

The suspension unloading resulted in a 48.07±6.43 g weight loss and a Wb:Wm ratio of 4.37±0.16 for the AL. This ratio was in agreement with that of Cosmos 2044 HSU and control muscles (unpublished data, D.A. Riley: HSU: 4.43±0.20; control: 3.34. ±0.14). Following ECCON treatment, Poi-drop was -17.8± 4.2 %Poi. The ECCON treatment also produced an initial cycle mean prestretch tension (Ppre-str) of 46.5±6.1 %Poi and a mean endstretch tension (Pend-str) of 166.5±4.9 %Poi. See Figure **2** for physiological parameter location on the illustrated tension trace diagram.

Physiological Parameters Vs. Lesion Density Relationships

The relationships of the initial cycle physiological parameters vs. lesion density and lesion density by type are provided in Table **1**. Ppre-str as %Poi was highly related to lesion density ($R^2 = 0.99$), as was dPtetanic/dt (R^2=0.93). In agreement with previous findings, "Work" demonstrated a relatively high correlation to lesion density (R^2=0.842). The posttreatment decrease in Poi (Poi-drop) was less tightly correlated with lesion density (R^2=0.59), as was the dP(stretch)/dt (R^2=0.40). Among the least related parameter to lesion density was Pend-str Wb:Wm ratio ($R^2 \leq 0.017$).

Table 1. Correlation of various physiological parameters[a] with lesion density or pooled lesion density by type (WID-A + OPAQ)[b] and (MIS-A + HS)[c]

Parameter[a]	**rs**[d]	**R^2** [f]

Tension, Pbeg-str (% maximum)	1.000[e]	0.950
Tension, Pbeg-str (% Poi)	1.000[e]	0.994
Tension, Pbeg-str (% Poi)[b]	1.000[e]	0.993
Tension, Pbeg-str (% Poi)[c]	1.000[e]	0.982
Tension, Pend-str (% Poi)	−0.182	0.017
dP (tetanic)/dt (g/sec/100 mg)	0.917[e]	0.926
dP (stretch)/dt (g/sec/100 mg)	0.ND[g]	0.399
Work (g-cm/100 mg muscle)	0.750	0.842
Poi drop, postECCON (% Poi)	0.917[e]	0.596
Poi drop, postECCON (g/100 mg muscle)	0.917[e]	0.731
Wb:Wm ratio (g/mg)	0.083	0.016

[a] Parameter in the initial cycle of ECCON treatment was plotted against lesion density or "pooled lesion density by type."[bc] the distal tendon of one animal released 1.5 min into the test was reattached and the test reinitiated for a total of 6.5 min. As the initial Poi was probably underestimated and the total treatment time was longer, this animal was excluded from the correlational data (n = 5). The "lesion density" value for this animal was within the range of the other five, so it was included in the group means (n = 6/group).

[b] "Pooled lesion density by type (WID-A + OPAQ)" vs. P(beg-str) correlational data.

[c] "Pooled lesion density by type (MIS-A + HS)" vs. P(beg-str) correlational data.

[a, d] Spearman's Rank Correlation Coefficient (Range: +1 to −1; indicates degree of agreement between two ranks).

[e] Reject null hypothesis that the physiologic parameter is independent of "lesion density" or "pooled lesion density by type" ($Z > 1.96$, $P < 0.05$; Zar, 1974).

[f] The square of the correlation coefficient describing the least square line ($y = ax + b$). Represents the degree to which the parameter explains the variation in "lesion density" or "pooled lesion density by type." (Perfect correlation: 1.00; Zar, 1974.)

[g] ND/not determined, as R^2 value was low.

DISCUSSION

The ECCON treatment of atrophic rodent AL muscles resulted in five morphological types of sarcomere lesions evident at the light microscopic level, which were completely absent from the SHAM samples and greatly diminished in the NonECCON-treated samples. Absence of lesions from SHAM samples processed identically to both ECCON and NonECCON groups argues strongly against muscle processing as causal in lesion production. The implications of each the five lesion types to a lesion formation mechanism are discussed below, followed by a plausible lesion formation sequence, considering the light morphology, myosin immunostaining characteristics and ultrastructure of the lesion types. Lastly, the implications of the tension parameters vs. lesion density correlations are discussed.

Mechanistic Implication of the Individual Lesion Types

Lesions are discussed in order of increasing sarcomere deform ratios (SDR): FC to WID-A to OPAQ to MIS-A to HS.

The presence of the FC lesion type morphologically supports that localized loss of calcium homeostasis is involved in FC lesion development and possibly in the initial stages of the proposed lesion sequence (elevated internal Ca^{++}, released from either sarcoplasmic reticulum or mitochondria; and extracellular Ca^{+}, via sarcolemma or T-tubule damage). Elevated Ca^{++} is suggested by the hypercontraction, and protease activation is suggested by the patchy loss of contractile proteins and Z-line components (Duncan, **1987**). That FC lesions are an early development is implied by the minimal reduction of myosin immunostaining in the FC lesion type relative to that seen in the MIS-A and HS lesion types, as well as retention of the contractile ability (the lesioned

sarcomeres are contracted). Similar lesions have been reported following a single eccentric contraction applied to whole EDL muscle and single fibers of the soleus and EDL (Hunter and Faulkner, **1996**; MacPherson et al., **1996**). FC lesions may be an entry route directly to MIS-A and HS lesions (highest Ca^{++}, most severe FC lesions, greatest proteolysis and cytoskeletal digestion), or via formation of WID-A lesions (lower Ca^{++}, very mild FC lesions, mild proteolysis and cytoskeletal protein nicking; see WID-A, below).

WID-A lesions are among the most interesting of the five types, because the sarcomere disorganization is consistent with thick filament lateral displacement from the A-band into the I-band prior to extensive Z-line destruction. This contradicts previous investigations concluding that Z-lines are the first site of sarcomere failure (Z-line streaming), i.e., the so-called “Achilles' heel” of the sarcomere. Marked Z-line streaming was reported in type IIB fibers (FG, fast twitch, glycolytic) of man following intense exercise (Friden et al., **1983**), suggesting a differential Z-line susceptibility across fiber type. However, the presence of WID-A lesions morphologically support failure of the “thick-filament-centering protein,” titin, as a primary event in lesion onset, prior to excessive Z-disk disruption in the atrophic slow twitch region of the AL. That the WID-A lesions occur early in the proposed progression sequence is inferred by the relatively intact Z-lines and thick filaments, as well as deformation ratios (SDR) close to unity. Single eccentric contractions of soleus (1.4 Lo) and extensor digitorium longus (1.1 Lo) muscle fibers show the initial stages of thick filament slippage (MacPherson et al., **1996**). Absence of M-lines within this lesion type implies that central crosslinks binding the thick filament in register are also disrupted as WID-A lesions form. WID-A lesions are similar to the sarcomere disruptions described for dystrophic muscle (Cullen et al., **1992**), and genetically normal muscle in which titin had been denatured by exposure of living muscle to X-rays. Titin destruction was confirmed by either the absence or diminished presence of the titin bands after denaturing gel electrophoresis (Horowits et al., **1986**).

The observation of transitional morphologies between WID-A and OPAQ lesion types, consisting of displaced thick filaments and larger SDRs, indicate that as WID-A lesions involve more sarcomeres and become more stretched, OPAQ lesions are generated. Patches of missing (degraded) and laterally slipped thick filaments observed in OPAQ lesions suggest increasing proteolysis occurs within this lesion type and leads to the more hyperstretched lesion types: MIS-A and HS.

The progressive thick filament slippage of the MIS-A and HS lesion types, streaming Z-disk remnants, and general digested appearance, which is paralleled by the progressive loss of myosin immunostaining of these lesions, as the LDR and SDR values increase, suggests that the MIS-A and HS lesions develop toward the end of our proposed lesion progression sequence. In severe cases such enlarged SDR values would indicate danger of sarcolemmal tearing leading to segmental necrosis and mononuclear cellular invasion, as reported 3 days following the fastest strain rate of the three eccentric contraction protocols pioneered by McCully and Faulkner (**1986**; strain, 0.2 Lf beginning at 0.9 Lf; strain rate, 1.0 Lf/s; Lf is optimal muscle fiber length, as opposed to optimum muscle length, Lo).

Mechanistic Implications of the Collective Myofibrillar Lesion Types

When collectively viewed, the most striking ultrastructural observation of the present study was the presence of thick filament lateral displacement in most of the lesion types. The increasing degrees of thick filament slippage at the EM level across the lesion types (FC << WID-A < OPAQ << MIS-A << HS) paralleled the LDR increases at the LM level across lesion types (FC << WID-A ≤ OPAQ ≤ MIS-A < HS). That lateral slippage of the thick filaments was involved was confirmed by lesion type ultrastructure. This suggests the five lesion types seen in LM level semithin sections were actually stages in a progression with either of the following two scenarios: 1) FC to [WID-A to OPAQ] to MIS-A to HS, or 2) FC to MIS-A to HS. Interestingly, myosin immunostaining intensity across the lesion types support the latter sequence with a similar order (most to least intensity): FC > MIS-A >> HS. The degree of immunostaining loss across these three lesion types is explained as the myosin containing thick

filaments spread over the widening sarcomere. However, for the WID-A and OPAQ lesions, the almost absent myosin immunoreactivity was not accompanied by a parallel loss in toluidine blue staining, histochemically indicating an A-band component presence (probably myosin) not detected by immunostaining. This difference may be reconciled by assuming that displaced thick filaments tightly interact with actin and introduce reversible steric hindrance to antibody penetration and immunomyosin detection in the WID-A lesion. A second potential explanation is that the myosin epitopes in this densely packed lesion type are blocked by accumulation of other protein adducts such as ubiquitination. We have unpublished results demonstrating intense immunolocalization of ubiquitin-conjugates to sarcomere lesions (D.A. Riley, unpublished communications). The increase in polyribosomes within the lesions are indicative of focal protein synthesis and assembly. Such polyribosomes are also visible in MIS-A lesions from the ECCON-treated muscle.

Lesion Progression Entry Points: FC Vs. WID-A

It remains to be determined whether the morphologically supported failure of titin results from mechanical breakage via excessive specific tension, structural failure via protease nicking, or a combination of these processes to generate WID-A lesions. In the present study, the intact Z-lines of this lesion type mitigate against excessive proteolysis and, thus, argue against WID-A lesion development from severe FC lesions. However, titin is among the most sensitive of the sarcomere proteins to proteolysis (Matsumura et al., **1989**). Involvement of calcium-dependent protease in sarcomere lesion formation is strongly suggested by the reduction of lesions with calpain inhibitors in other studies (Duan et al., **1990**). Should titin be nicked, this would lead to a decreased or unequal elastic “thick-filament-centering” force across an individual sarcomere, along sarcomeres in series, and across myofibrils in parallel. If proteolysis were mild, titin nicking could proceed in a transient mild FC lesion, which could develop into a WID-A lesion with relatively intact Z-disks, during subsequent contractions. Whether FCs precede WID-As and OPAQs would largely depend on the local Ca^{++} concentration. High Ca^{++} should generate severe FC lesions with high protease activity bypassing the WID-A lesion type, whereas lower Ca^{++} could produce very subtle FC lesions and mildly nicked titin strands leading to the formation of a WID-A lesion with loading. Because there are six titin strands per myosin thick filament (Wang, **1985**), it is highly likely that mild proteolytic nicking of a single strand would produce uneven elastic forces across the sarcomere, but have enough remaining elasticity to prevent excessive sarcomeric stretch, as seen in WID-A lesions. With continued eccentric insult these remaining strands should gradually give way, producing the lesion types with the higher SDR values. However, excessive proteolytic activity (severe FC lesion) should lead to catastrophic failure of titin and complete bypass of the WID-A/OPAQ lesion types directly to the MIS-A/HS lesion types.

Implications of Lesion Density Vs. Physiological Parameters

The ECCON-treated muscles demonstrated a very wide variation in lesion density and lesion density by type, despite the relatively narrow endstretch tensions (Pend-str, 150–170 %Poi). This level of variability was also mirrored in the Cosmos 2044 spaceflight rats in that the percentage of fibers affected ranged between 17% and 70% over similar reload times. However, individual rat behavior was highly variable (Riley et al., **1992**). Despite this wide variation, both lesion density and pooled lesion density by type correlate highly with Ppre-str levels as (%Poi) and explain at least 98% of the variation in lesion density. The initial rate of tension rise during tetanus (dPtetanic/dT) also correlates very highly with lesion density, and is in keeping with the previous reports that within the anatomical range muscles are not damaged unless they contract (Irintchev and Wernig, **1987**), and our previous observations that myofibrillar lesions are a reload phenomena (Riley et al., **1995**, **1996**). Tight linkage with Ppre-str predicts a closer grouping in lesion density if a longer delay in the tetanic contraction prior application of the ECCON treatment were used. A lack of correlation with the Wb:Wm ratio is indicative that the ECCON treatment is predominantly responsible for lesion formation, as opposed to the 3–4 hr reload period following the ECCON treatment, during which the rats showed minimal movements as they recovered from anesthesia. Nonetheless, the 7-hr postECCON sampling period allowed time for progression of sarcomere lesions

to occur to varying degrees and manifest what appears to be multiple stages of lesion development in a single muscle.

Previous studies have emphasized the posttreatment loss of maximal tension (Poi-drop) following eccentric treatment as the principal indicator of eccentric muscle damage (MacPherson et al., **1996**; Lieber and Friden, **1993**; Lieber et al., **1991**, Warren et al., **1993a**,**b**, **1994**). In light of the present data showing a poorer correlation of lesion density and Pend-str or Poi-drop, this may not be the best indicator of eccentric myofibrillar damage, although it is certainly the simplest and quickest "damage" parameter to monitor. It should be noted here that loss of tension is the least informative "damage" parameter when exploring mechanism of muscle breakdown (susceptible sarcomeric components: Z-disks, cytoskeleton, thick filaments; susceptible myofiber components: sarcolemmal vs. sarcomeric). These findings stress the importance of determining fine structure and ultrastructure of posttreated muscle, and of obtaining a complete tension record during treatment, not just the peak tension or endstretch tension for determining the role of tension (stress) in myofibrillar eccentric lesion development at a specified length increase (strain).

The Ppre-str correlation with lesion density is consistent with the previously proposed "critical tension level," past which damage ensues, and is not necessarily related to the treatment maximum tension or endstretch tension. In the Lieber and Friden (**1993**) study the treatment producing the maximum Pend-str, ("late stretch"), was not the treatment that produced the greatest work, ("early stretch"). More recently, Faulkner's laboratory (Hunter and Faulkner, **1996**) reported the highest correlation with damage, as assessed by declining Poi, is the work done by the muscle; this is consistent with the present findings ("work" explained 84% of variance in "lesion density"). An implication of the increased Ppre-str correlation to lesion density is that with increases in Ppre-str and increased crossbridge formation, the muscle spends more time contracted above a critical tension level, while being required to actively lengthen and break more crossbridges. It is this active crossbridge breaking in pliometric contractions that requires more tension, which we view as the damaging factor.

Additionally, at longer sarcomeric lengths a greater percentage of the muscle tension is generated by stretching the elastic titin (Wang et al., **1991**; Horowits et al., **1992**). Thus, greater dependence is placed on the "thick-filament-centering" function of titin in the descending limb of the length tension curve. If titin elasticity is uneven or depressed (via protease nicking) in HSU muscle, the sarcomeric length inhomogeneities characteristic of lengthening contractions in normal single muscle fiber model would be exacerbated in the pliometrically contracting HSU muscle. Under this condition, increased numbers of the sarcomeres could lengthen to the unstable condition past Lo, as suggested by Morgan (**1990**; Lynn and Morgan, **1994**), leading to lesion development and growth. Such a situation would be worsened should the tension generating crossbridges be unequal across many individual atrophic sarcomeres. We have observed localized reductions in actin and actin-myosin packing density as a result of 17 days of bedrest in humans (Widrick et al., **1997**; Riley et al., **1998**). Such alterations in packing density may suggest an exaggerated imbalance in the force-producing units across many individual atrophic sarcomeres. Theoretically, if compromised titin elasticity and exaggerated sarcomeric force instability across many individual sarcomeres were achieved in combination in HSU muscle, this event should prove devastating to sarcomeric integrity.

It is interesting to note that the ultrastructure of all lesions surveyed in semithin sections described in the present study could be predicted by differing levels of titin failure at the EM level. For example: FCs show minimal titin failure and thick filament slippage, and Ca^{++} activated protease to a varying extent, acting on titin and Z-disks in hypercontracted sarcomeres; WID-As imply unequal titin elasticity on either side of 1–2 sarcomeres of relatively normal stretch; OPAQs show more Z-disk disruption as weaker or unequal titin filaments allow contracting muscle to pull Z-disk apart (slightly hyperstretched), with greater thick filament slippage over 2–5 or so sarcomeres; MIS-As show areas (1–18 sarcomeres) of intermittently misaligned thick filaments and moderately hyperstretched Z-line remnants mixed with relatively intact sarcomeres; HSs show

large areas 1–16 sarcomeres of severely hyperstretched regions, drastically slipped thick filaments, and completely disrupted Z-line remnants extending uniformly throughout the lesion.

Summary of ECCON Protocol and High-Resolution Lesion Protocol Usefulness

Previous reloading studies indicate that atrophic postural muscles show increased susceptibility to eccentric treatment (Riley et al., **1992**, **1995**, **1996**; Warren et al., **1994**) and suggested a differential lesion response across fiber types between normal and atrophic muscle. An adaptation of the immunomyosin technique presented here allows for fiber type determination in serial semithin sections (Thompson, Vijayan, and Riley, submitted) and, thus, a means to identify a lesion susceptible fiber type in reload damage (Vijayan, Thompson, and Riley, **1998**). Also, the present eccentric stimulation method produced lesions morphologically similar to those observed following HSU and postflight reloading damage in rats, (Riley, **1990**, **1992**; Krippendorf and Riley, **1994**) suggesting parallel mechanisms. Three of the five lesion types (WID-A, MIS-A, and HS) presently reported have also been described in eccentrically challenged human muscle (Gibala et al., **1995**). The FC, WID-A/OPAQ, and MIS-A types have been reported in eccentrically challenged frog, rat, and human muscle (Lieber et al., **1991**; Riley et al., **1992**; Wood et al., **1993**). Thus, the present model produces damage in rats which may be extrapolated to HSU-reloaded rats, as well as to eccentrically loaded human muscle. The capability to successfully reattach the rodent AL tendon enables study of the time course of lesion development/repair in postural muscle, and is not limited to the study of lesion formation with known muscle tension immediately following the eccentric treatment. Perfusion fixation at fixed joint angles in this rat model allows determination of sarcomeric length at various joint angles within the anatomical range of this muscle. Sarcomeric length across the anatomical range of muscles in humans is practically impossible to determine from needle punch muscle biopsy samples and would require very invasive surgical intervention to clamp muscles at fixed joint angles prior to sampling and fixation. Thus, the rodent model allows use of more invasive, but much more informative protocols for studying lesion formation and lesion prevention that are applicable to the human model. A key question in HSU muscle is not so much whether “strain” is a more important damage factor than “stress,” as is believed by Lieber and Friden (**1993**), but whether eccentrically challenged atrophic muscle at a given “strain” may be more severely damaged by less “stress” or specific tension than in normal muscle. This very important basic question between “normal” and “chronically unloaded” muscle has yet to be answered, and the described ECCON protocol and high-resolution lesion characterization technique are crucial to this determination.

Acknowledgements

Immunomyosin and electron microscopy protocols were performed by JLT and supported in part by Institutional Biomedical Sciences Research Support Grant #92-F001 to JLT; eccentric protocols were performed by JLT and EMB at Marquette University partially under NASA grant NAG5–6058 to RHF; electron microscopy was performed at the EM Core Facility, MCW partially under NASA grant NAG2–956 and NIH grant U01NS33472 to DAR; the anatomical drawing of the rodent AL was done by Carolyn Snyder, and the computer programming for the ECCON protocol was done by Dr. Thomas Trusk. Portions of this work were presented at the 1996 meeting of the American College of Sports Medicine.

References

Armstrong RB, Phelps RO. 1984. Muscle fiber type composition of the rat hindlimb. *Am J Anat* **171**: 259– 272.

Armstrong RB, Ogilvie RW, Schwane JA. 1983. Eccentric exercise-induced injury to rat skeletal muscle. *J Appl Physiol* **54**: 80– 93.

Brooks SV, Zebra E, Faulkner JA. 1995. Injury to muscle fibers after single stretches of passive and maximally stimulated mucles in mice. *J Physiol* **488**: 459– 469.

Cullen MJ, Fulthorpe JJ, Harris JB. 1992. The distribution of desmin and titin in normal and dystrophic human muscle. *Acta Neuropathol* **83**: 158– 169.

Duan C, Delp MD, Hayes DA, Delp PD, Armstrong RB. 1990. Rat skeletal muscle mitochondrial [Ca^{++}] and injury from downhill walking. *J Appl Physiol* **68**: 1241– 1251.
Duncan CJ. 1987. Role of calcium in triggering rapid ultrastructural damage in muscle: A study with chemically skinned fibers. *J Cell Sci* **87**: 581– 594.
Duncan CJ. 1989. Mechanisms that produce rapid damage to myofilaments of amphibian skeletal muscle. *Muscle Nerve* **12**: 210– 218.
Fitts RH, Metzger JM, Riley DA, Unsworth BR. 1986. Models of disuse: A comparison of hindlimb suspension and immobilization. *J Appl Physiol* **60**: 1946– 1953.
Friden J, Lieber RL. 1992. Structural and mechanical basis of exercise-induced muscle injury. *Med Sci Sports Exerc* **24**: 521– 530.
Friden J, Sjostrom M, Eklblom B. 1983. Myofibrillar damage following intense eccentric exercise in man. *Int J Sports Med* **4**: 170– 176.
Friden J, Seger J, Ekblom B. 1988. Sublethal muscle fibre injuries after high-tension anaerobic exercise. *Eur J Appl Physiol* **57**: 360– 368.
Gibala MJ, MacDougall JD, Tarnopolsky MA, Stauber WT, Elorniaga A. 1995. Changes in human skeletal muscle ultrastructure and force production after acute resistance exercise. *J Appl Physiol* **78**: 702– 708.
Hargens AR, Parazynski S, Aratow M, Friden J, 1989. Muscle changes with eccentric exercise: Implications on Earth and in Space. In: G Benzi, editor, 2nd Ed. Nice, France: J Libbey Eurotext Ltd 299– 312.
Horowits R. 1992. Passive force generation and titin isoforms in mammalian skeletal muscle. *Biophys J* **61**: 392– 398.
Horowits R, Kempner ES, Bisher ME, Podolsky RJ. 1986. A physiological role for titin and nebulin in skeletal muscle. *Nature* **323**: 160– 164.
Hunter KD, Faulkner JA, 1996. Injury to single muscle fibers by single pliometric contractions: Role of initial fiber length. *Med Sci Sports Exerc* **28**: S188– 1118.
Hutchins MO, Skjonsby HS. 1990. Microtrauma to rat superficial masseter muscles following lengthening contractions. *J Dent Res* **69**: 1580– 1585.
Irintchev A, Wernig A. 1987. Muscle damage and repair in voluntarily running mice: Strain and muscle differences. *Cell Tissue Res* **249**: 509– 521.
Krippendorf BB, Riley DA. 1994. Temporal changes in sarcomere lesions of rat adductor longus muscles during hindlimb reloading. *Anat Rec* **238**: 304– 310.
Lieber RL, Bodine-Fowler SC. 1993. Skeletal muscle mechanics: Implications for rehabilitation. *Phy Ther* **73**: 844/25– 856/37.
Lieber RL, Friden J. 1993. Muscle damage is not a function of muscle force but active muscle strain. *J Appl Physiol* **74**: 520– 526.
Lieber RL, Woodburn TH, Friden J. 1991. Muscle damage induced by eccentric contractions of 25% strain. *J Appl Physiol* **70**: 2498– 2507.
Lynn R, Morgan DL. 1994. Decline running produces more sarcomeres in rat vastus intermedius muscle fibers than does incline running. *J Appl Physiol* **77**: 1439– 1444.
MacPherson PCD, Schork MA, Faulkner JA, 1996. Contraction-induced injury to single fiber segments from fast and slow muscles of rat by single stretches. *Am J Physiol* **271**: C1438– C1446.
Matsumura K, Shimizu T, Mannen T. 1989. In vitro degradation of the Duchenne muscular dystrophy gene produce (dystrophin). *Biomed Res* **10**: 325– 328.
McCully KK, Faulkner JA. 1985. Injury to skeletal muscle fibers of mice following lengthening contractions. *J Appl Physiol* **59**: 119– 126.
McCully KK, Faulkner JA. 1986. Characteristics of lengthening contractions associated with injury to skeletal muscle fibers. *J Appl Physiol* **61**: 293– 299.
Morgan DL. 1990. New insights into the behavior of muscle during active lengthening. *Biophys J* **57**: 209– 221.
Newham DJ, McPhail G, Mills KR, Edwards RHT. 1983. Ultrastructrual changes after concentric and eccentric contractions of human muscle. *J Neurol Sci* **61**: 109– 122.

Ogilvie RW, Armstrong RB, Baird KE, Bottoms CL. 1988. Lesions in the rat soleus muscle following eccentric biased exercise. *Am J Anat* **182**: 335– 346.

Popesko P, Rajtova V, Horak J, 1990. *A Colour Atlas of the Anatomy of Small Laboratory Animals*, Vol **II**. London, England Wolfe Publishing, Ltd., 14, 79– 80, 86–89.

Riley DA, Ilyina-Kakueva EI, Ellis S, Bain JLW, Slocum GR, Sedlak FR. 1990. Skeletal muscle fiber, nerve, and blood vessel breakdown in space-flown rats. *FASEB J* **4**: 84– 91.

Riley DA, Ellis S, Giometti CS, Hoh JFY, Ilyina-Kakueva EI, Oganov VS, Slocum GR, Bain JLW, Sedlak FR. 1992. Muscle sarcomere lesions and thrombosis after spaceflight and suspension unloading. *J Appl Physiol* **73**: 33S– 43S.

Riley DA, Thompson JL, Krippendorf BB, Slocum GR. 1995. Review of spaceflight and hindlimb suspension unloading induced sarcomere damage and repair. *BAM* **5**: 139– 145.

Riley DA, Ellis S, Slocum GR, Sedlak FR, Bain JLW, Krippendorf BB, Lehman CT, Macias MY, Thompson JL, Vijayan K, DeBruin JA. 1996. In-flight and postflight changes in skeletal muscles of SLS-1 and SLS-2 spaceflown rats. *J Appl Physiol* **81**: 133– 144.

Riley DA, Bain JLW, Thompson JL, Fitts RH, Widrick JJ, Trappe SW, Trappe TA, Costill DL. 1998. Disproportionate loss of thin filaments in human soleus muscle after 17-day bedrest. *Muscle Nerve* **21**: 1280– 1289.

Roy RR, Hirota WK, Kuehl M, Edgerton VR. 1985. Recruitment patterns in the rat hindlimb muscle during swimming. *Brain Res* **337**: 175– 178.

Schwane JA, Armstrong RB. 1983. Effect of training on skeletal muscle injury from downhill running in rats. *J Appl Physiol* **55**: 969– 975.

Sjostrom M, Friden J. 1984. Muscle soreness and muscle structure. *Med Sports Sci* **17**: 169– 186.

Thompson JL. 1993. Sarcomere lesions in atrophied reloaded adductor longus. *NASA Tech Memo* **4501**: 250– 253.

Thompson JL, 1994. Sarcomere lesions in atrophied reloaded adductor longus. *NASA Tech Memo* 304– 308.

Vijayan K, Thompson JL, Riley DA. 1998. Sarcomere lesion damage occurs mainly in slow fibers of reloaded rat adductor longus muscles. *J Appl Physiol* **85**: 1017– 1023.

Wang K. 1985. Sarcomere-associated cytoskeletal lattices in striated muscle. Review and hypothesis. *Cell Muscle Motil* **6**: 315– 369.

Wang K, McCarter R, Wright J, Beverly J, Ramirez-Mitchell R. 1991. Regulation of skeletal muscle stiffness and elasticity by titin isoforms: A test of the segmental extension model of resting tension. *Proc Natl Acad Sci USA* **88**: 7101– 7105.

Warren GL, Hayes DA, Lowe DA, Prior BM, Armstrong RB. 1993a. Materials fatigue initiates eccentric contraction-induced injury in rat soleus muscle. *J Physiol* **464**: 477– 489.

Warren GL, Hayes DA, Lowe DA, Armstrong RB. 1993b. Mechanical factors in the initiation of eccentric contraction-induced injury in rat soleus muscle. *J Physiol* **464**: 457– 475.

Warren GL, Hayes D, Lowe DA, Williams JH, Armstrong RB. 1994. Eccentric contraction-incuded injury in normal and hindlimb-suspended mouse soleus and EDL muscles. *J Appl Physiol* **77**: 1421– 1430.

Watchko JF, Johnson BD, Gosselin LE, Prakash YS, Sieck GC. 1994. Age-related differences in diaphragm muscle injury after lengthening activations. *J Appl Physiol* **77**: 2125– 2133.

Widrick JJ, Romatowski JG, Bain JLW, Trappe SW, Trappe TA, Thompson JL, Costill DL, Riley DA, Fitts RH, 1997. Effect of 17 days of bed rest on peak isometric force and unloaded shortening velocity of human soleus fibers. *Am J Physiol* **273**: C1690– C1699.

Wood SA, Morgan DL, Proske U, 1993. Effects of repeated eccentric contractions on structure and mechanical properties of toad sartorius muscle. *Am J Physiol* **265**: C792– C800.

Zar JH, 1974. *Biostatistical Analysis*. Englewood Cliffs, NJ: Prentice Hall. p 109– 114.